Single-Frequency Amplitude-Modulation Sensor for Dielectric Characterization of Solids and Microfluidics

Paris Vélez, *Member*, *IEEE*, Jonathan Muñoz-Enano, Amir Ebrahimi, *Member*, *IEEE*, Cristian Herrojo, *Member*, *IEEE*, Ferran Paredes, *Member*, *IEEE*, James Scott, *Member*, *IEEE*, Kamran Ghorbani, *Senior Member*, *IEEE*, and Ferran Martín, *Fellow*, *IEEE*

***Abstract*— A microfluidic sensor based on a microstrip line loaded with a composite resonator is reported in this paper. The composite resonator combines a shunt connected step impedance resonator (SIR) and a complementary split ring resonator (CSRR) etched in the ground plane. By etching the CSRR beneath the patch of the SIR, the composite CSRR-loaded SIR resonator exhibits two transmission zeros and a pole in between. The operating principle of the sensor is the variation of the transmission coefficient at the pole frequency of the bare resonator, when a material or liquid under test (LUT) is in contact with the CSRR (the sensitive element). By designing the CSRR-loaded SIR resonator with closely spaced pole and transmission zeros, highly sensitive sensors are obtained. Despite the fact that the proposed sensor can also operate as a frequency variation sensor, using it as a single-frequency sensor based on the variation of the transmission coefficient (caused by the LUT) at a specific frequency reduces sensor costs. The reason is that a harmonic signal injected to the input port of the microstrip-based sensor plus a simple amplitude modulation (AM) detector (connected to the output port) suffices for measuring purposes. The proposed microfluidic sensor is applied to the characterization of volume fraction of solutions of isopropanol in deionized (DI) water. The sensor is able to resolve volume fractions as small as 5%, and the maximum measured sensitivity is as good as 4 mV/%.**

***Index Terms*— Complementary split ring resonator (CSRR), microfluidics, microstrip technology, microwave sensors, permittivity measurements, step impedance resonator (SIR).**

I. Introduction

IN MODERN life, within the paradigm of the internet of things (IoT), or internet of everything (IoE), there is an increasing demand for sensors and sensor networks. Applications include the measurement of variables of interest (e.g., related to environmental phenomena), the assistance to elderly and disabled people, the control and monitoring of industrial processes, and the improvement of the quality of life and energy management in the so-called smart home, among others. Most currently available sensors are based on optical and photonic technologies (image sensors, optical fiber sensors, wearable chemical and biological sensors, laser-based sensors, and nanophotonic biosensors, are some examples of optical/photonic sensors). Nevertheless, the research in the field of microwave sensors has experienced a significant growth in recent years, particularly in the area of material characterization and analysis. The main reason is related to the fact that microwaves are very sensitive to the properties of the materials to which they interact. Additionally, microwave technology exhibits interesting properties for sensing, including low-cost generation and detection systems, interaction to the materials at different scales (i.e., through the near-field or the far-field), compatibility with planar technology, wireless connectivity, and robustness against harsh environments, among others. These properties are useful for the implementation of highly sensitive, low-cost, small size, low-profile, and robust microwave sensors and wireless sensors, which can compete against their optical counterparts, in a number of specific areas (such as material sensing).

Within the area of material sensing (including solids and liquids), planar microwave resonant sensors have attracted the interest of many researchers. On one hand, as compared to bulk sensors (e.g., cavity sensors or waveguide-based sensors [1],[2], among others), planar sensors exhibit low profile and low cost, necessary attributes in many applications (e.g., conformal sensors [3], wearable sensors [4], submersible sensors [5], integrated sensors [6], lab-on-a-chip sensors [7], microfluidic sensors [8]-[11], etc.). On the other hand, the resonance frequency, phase and quality factor of electrically small planar resonators are, in general, very sensitive to the

This work was supported by MINECO-Spain (projects TEC2016-75650-R and PID2019-103904RB-I00), Generalitat de Catalunya (project 2017SGR-1159), Institució Catalana de Recerca i Estudis Avançats (who awarded Ferran Martín), and by FEDER funds. J. Muñoz-Enano acknowledges Secreteraria d'Universitats i Recerca (Gen. Cat.) and European Social Fund for the FI grant. Paris Vélez acknowledges the Juan de la Cierva Program for supporting him through Project IJCI-2017-31339.

P. Vélez, J. Muñoz-Enano, F. Paredes, C. Herrojo and F. Martín are with GEMMA/CIMITEC, Departament d'Enginyeria Electrònica, Universitat Autònoma de Barcelona, 08193 Bellaterra, Spain (e-mail: Ferran.Martin@uab.es).

A. Ebrahimi, J. Scott and K. Ghorbani are with the School of Engineering, Royal Melbourne Institute of Technology (RMIT University), Melbourne, VIC 3001, Australia (e-mail: amir.ebrahimi@rmit.edu.au). .

properties of their surrounding medium. Such high sensitivity and their small size make these resonators very interesting for material sensing and material composition determination. Nevertheless, planar sensors based on electrically small resonators have also been applied to the measurement of spatial variables [12]-[27]. It should also be mentioned that non-resonant planar sensors devoted to material characterization have been reported [28]-[30]. The working principle of most of these sensors, based on meander [30] or artificial lines [28], is phase variation caused by a change in the permittivity of the material under test. Although the reported phase variation sensors exhibit high sensitivities, the main limitation of these sensors is their size (note that the phase of an ordinary or artificial line incurs a stronger variation as its length increases).

Most reported planar microwave resonant sensors can be divided into four main categories, i.e., frequency variation sensors [12],[31]-[46], frequency splitting sensors [21],[47]-[55], coupling modulation sensors [13]-[24],[56], and differential-mode sensors [28],[30],[57]-[69]. In frequency variation sensors, sensing is based on the variation of the resonance frequency and peak (or notch) magnitude of the frequency response of a transmission line loaded with the sensing resonant element, caused by the variation in the permittivity of the material under test. Frequency variation sensors are very simple, small, and cost effective, since a single resonant element suffices for sensing. However, these sensors are subjected to cross sensitivities related to potential changes in environmental factors (e.g., temperature and humidity). To alleviate the effects of ambient conditions, symmetry based sensors [70],[71] constitute a good solution, as far as symmetry is invariant under environmental changes, at least at the typical scale of the sensors.

Among symmetry based sensors, coupling modulation sensors are implemented by symmetrically loading a line with a symmetric resonator. A necessary condition for sensing using this approach is that the symmetry planes of the considered line and resonator should be of different electromagnetic sort, i.e., one a magnetic wall and the other one an electric wall [70]. Thus, perfect symmetry prevents line-to-resonator coupling, and the line is transparent. By contrast, by disrupting symmetry, e.g., by means of an asymmetric loading of the resonant element, or by means of a relative displacement between the resonator and the line, the coupling is activated, resulting in a notched response with magnitude intimately related to the level of asymmetry.

Frequency splitting sensors are also based on symmetry disruption. However, in these sensors, a transmission line is symmetrically loaded with a pair of (not necessarily symmetric) resonators. Under perfect symmetry, a single notch in the transmission coefficient arises, but such notch splits into two notches by symmetry truncation [70]. The differences in the notch frequencies and notch magnitudes are related to the level of asymmetry, typically caused by a different loading in the resonant elements (one loaded with the so-called reference sample, and the other one loaded with the sample under test).

Although frequency splitting sensors are conceptually similar to differential sensors, the latter use two independent sensing elements. The typical output variable in transmission line based differential sensors is the differential transmission coefficient, proportional to the so-called cross-mode transmission coefficient. The input variable in such sensors depends on the specific application. For material characterization and analysis, the typical input variable is the differential permittivity (between the reference sample and the sample under test), or the differential volume fraction (in measurements devoted to determine the solute content in liquid solutions).

One of the main limitations of frequency variation and frequency splitting sensors is the need to use a wideband interrogation signal for sensing, which increases the cost of the associated circuitry. By contrast, in coupling modulation and differential sensors, a single frequency suffices for sensing (unless two input variables, e.g. the real and the imaginary part of the permittivity, should be measured). For instance, in a recent paper [65], it was demonstrated that single frequency and two-port measurements in a differential microfluidic sensor are possible. Nevertheless, the measurement is restricted to obtaining the transmission coefficient at the operating frequency. The typical output variable in coupling modulation sensors is also the transmission coefficient measured at a certain frequency (usually the resonance frequency of the unloaded resonator).

In this paper, the main objective is to implement a single frequency sensor with a transmission coefficient highly sensitive to the dielectric constant of the material under test. For that purpose, a resonator-loaded line exhibiting at least one pole and one transmission zero closely spaced to the pole is needed. As it will be shown, these characteristics can be satisfied by using a composite resonator consisting of a step impedance resonator (SIR) combined with a complementary split ring resonator (CSRR) [72]. However, it is also our objective in the present paper to add an amplitude modulator (AM) detector to the output port of the transmission line based sensor, in order to consider the voltage amplitude of the output signal as the output variable of the sensor. By this means, a vector network analyzer generating a sweeping signal over a wide band is not needed for sensing, and sensor costs are reduced. Note that a simple harmonic oscillator, necessary to feed the transmission line based sensor, suffices for sensing, although its design is out of the scope of this paper (i.e., sensor feeding is carried out by means of a commercial instrument). It is important to highlight that in order to obtain high sensitivity, it is necessary to achieve a significant excursion of the transmission coefficient (at the operating frequency) when the dielectric constant of the material under test varies. However, it is also necessary that the maximum level of the transmission coefficient is close to 0 dB in order to obtain measurable voltage levels (without the need to use amplifier stages). For this main reason, the presence of a pole in the resonator-loaded line is convenient. By tuning the operating frequency of the sensor to the pole frequency of the bare sensor (or sensor loaded with a reference material), both

requirements (a significant excursion of the transmission coefficient and maximum value near 0 dB) are achieved, as it will be demonstrated. As a proof of concept demonstrator, the designed sensor is devoted to the characterization of volume fraction in solutions of isopropanol in DI water, and for that purpose, the sensor is equipped with a microfluidic channel and the necessary accessories (nevertheless, application to the characterization of solid samples is also considered in the paper).

The work is organized as follows. In section II, the typical topology of the sensor is presented, and its equivalent circuit model is reported and validated by parameter extraction and comparison between circuit and electromagnetic simulations. The working principle of the proposed sensor, based on the amplitude modulation of the feeding harmonic signal caused by changes in the dielectric constant of the material under test, is detailed in Section III. Section IV is devoted to the experimental validation, where first the sensor is devoted to the characterization of solid samples, and then it is equipped with a microfluidic channel in order to demonstrate its potential for the characterization of liquid samples (particularly, for the measurement of the volume fraction of isopropanol in solutions of DI water). A comparison to other approaches is included in Section V, where the advantages and limitations of the reported sensor are discussed. Finally, the main conclusions are highlighted in Section VI.

II. Topology and Circuit Model of the Proposed Sensor

The typical topology of the proposed sensor, excluding the necessary electronics for harmonic feeding and for obtaining the envelope function (AM detector), is depicted in Fig. 1(a), whereas Fig. 1(b) shows the equivalent circuit model (losses are neglected). The sensor consists of a microstrip line loaded with a shunt connected SIR (also known as step impedance shunt stub-SISS [73]), in turn loaded with a CSRR (etched in the ground plane). The combination of the SIR and CSRR behaves as a shunt composite resonator, described by the lumped reactive elements of Fig. 1(b). The SIR is modelled by the inductance L and the capacitance C, whereas L_c and C_c account for the CSRR. It should be mentioned that for the accurate description of the SIR by means of a lumped element circuit model consisting of a series LC resonator, as indicated in Fig. 1(b), it is necessary to have a high impedance contrast of the line sections forming the SIR resonator. For this reason, the inductive strip is very narrow, whereas the capacitive patch is wide. Note that, according to this model, the patch capacitance of the SIR should be entirely circumscribed within the inner metallic region of the CSRR, as illustrated in Fig. 1(a). The transmission line sections at both sides of the CSRR-loaded SIR are described by the characteristic impedance, Z_0, and by the electrical length kl, where k and l are the phase constant and physical length, respectively, of such line sections.

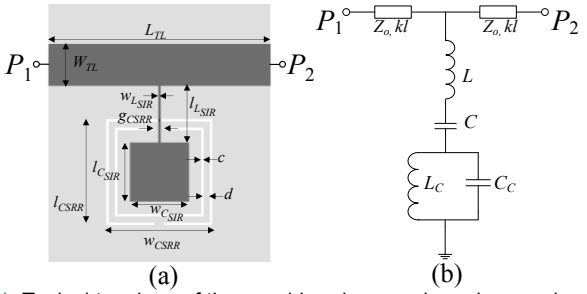

Fig. 1. Typical topology of the considered sensor based on a microstrip line loaded with a CSRR-loaded SIR resonator (a), and equivalent circuit model (b). Dimensions (in mm) are: l_{LSIR} = 4.6, l_{CSIR} = w_{CSIR} = 5.1, w_{LSIR} = 0.2, l_{CSRR} = 8.6, w_{CSRR} = 10.6, c = 0.2, d = 0.5, g_{CSRR} = 0.8, L_{TL} = 18, and W_{TL} = 3.4 (giving Z_0 = 50 Ω).

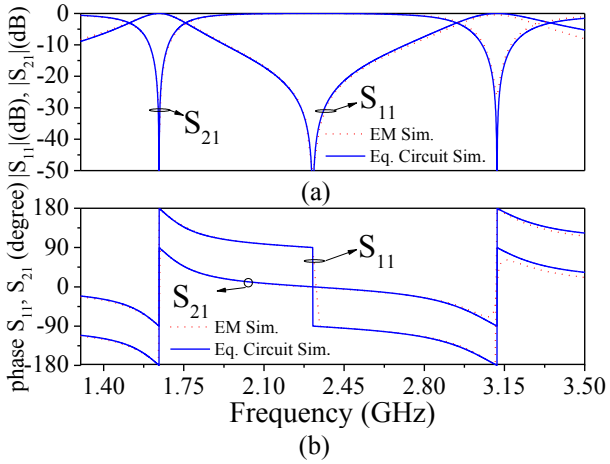

Fig. 2. Simulated frequency response of the transmission line loaded with the CSRR-loaded SIR resonator inferred from electromagnetic and circuit simulation by excluding losses. (a) Magnitude of the transmission, S_{21}, and reflection, S_{11}, coefficient; (b) phase of the transmission and reflection coefficient by excluding the access lines. The extracted lumped element values are L = 6.07 nH, C = 0.85 pF, L_c = 2.45 nH, and C_c = 1.92 pF.

By considering the dimensions indicated in the caption of Fig. 1 and the characteristics of the *Rogers 4003C* substrate with dielectric constant ε_r = 3.55 and thickness h = 1.524 mm, the frequency response of the structure of Fig. 1(a), inferred with *Keysight Momentum* by excluding losses, is the one depicted in Fig. 2. As it can be seen, the device exhibits two transmission zeros and a reflection zero (or pole) in between, as dictated by the Foster reactance theorem [74] (the second pole is at the origin, where the reactance of the shunt resonator opens). With the considered substrate parameters, the width of the microstrip line provides a characteristic impedance of Z_0 = 50 Ω.

For model validation, a parameter extraction procedure is necessary. Since the CSRR-loaded SIR resonator is described by four reactive elements, four conditions are needed to univocally determine such elements. The first condition is the pole (angular) frequency, given by

$$\omega_p = \frac{1}{\sqrt{L_c C_c}} \tag{1}$$

and directly inferred from the frequency response (at this frequency the shunt branch opens and the structure exhibits a

reflection zero where S_{11} is a minimum). Two additional conditions are given by the transmission zero (angular) frequencies, which are the two positive solutions of

$$\omega_z = \sqrt{\frac{LC + L_cC_c + L_cC \pm \sqrt{(LC + L_cC_c + L_cC)^2 - 4LCL_cC_c}}{2LCL_cC_c}} \quad (2)$$

Finally, the susceptance slope at the angular frequency of the pole, ω_p, provides the fourth condition. The susceptance slope is identical to the one of the L_cC_c parallel resonant tank, namely,

$$\left.\frac{dB}{d\omega}\right|_{\omega_p} = 2C_c \quad (3)$$

In order to obtain the susceptance slope, the admittance of the resonator ($Y = jB = Z^{-1}$) is inferred from the simulated S-parameters of the composite resonator with the ports directly connected to it (i.e., by excluding the access lines), according to [75]

$$Y = -\frac{2Y_0S_{11}}{1 + S_{11}} \quad (4)$$

where $Y_0 = 1/Z_0$.

The reactive element values of the considered resonator of Fig. 1(a) have been inferred from the indicated parameter extraction method (see the values in the caption of Fig 2). Figure 2 also includes the circuit response inferred from *Keysight ADS* using the extracted element values. The excellent agreement between the circuit and electromagnetic simulation responses for both the magnitude and the phase of the transmission and reflection coefficients validates the proposed circuit model and the parameter extraction procedure.

III. Working Principle for Sensing and Analysis

The sensing principle of the proposed sensor is the variation of the transmission coefficient caused by the presence of a material under test (either solid or liquid) in contact with the CSRR, the sensitive element. As compared to the response of the bare sensor, the frequency response shifts down when a material is in contact with the CSRR (obviously, the susceptance slope at the pole frequency also changes, due to the variation of the CSRR capacitance, C_c). Thus, the device can operate as a frequency variation sensor, where the output variable may be, e.g., the upper transmission zero frequency, or the pole frequency (the first transmission zero has been found to be less sensitive to the effects of the MUT, see Appendix A). However, as anticipated in the introduction, a wideband interrogation signal is necessary for sensing under this mode of operation.

Alternatively, the output variable may be the magnitude of the transmission coefficient at a certain frequency, f_0. In particular, by choosing $f_0 = f_{p,bare}$, the pole frequency of the bare sensor ($f_{p,bare} = \omega_{p,bare}/2\pi$), the transmission coefficient is expected to experience a significant variation by loading the CSRR with a MUT. Moreover, the transmission coefficient will be close to 0 dB for the bare sensor, and it progressively will decrease by increasing the dielectric constant of the MUT.

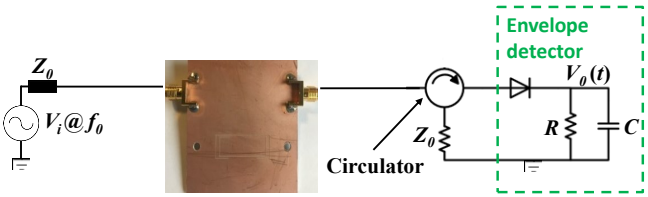

Fig. 3. Sketch of the proposed sensor, showing the working principle. The isolator (implemented by means of a circulator), cascaded between the output port of the sensor and the envelope detector, prevents from mismatching reflections from the diode.

Under these conditions, rather than the transmission coefficient, it is reasonable to consider the amplitude of the harmonic signal at the output port (in response to a harmonic interrogation signal) as the output signal of the sensor. Such signal can be inferred by means of an envelope detector, following a similar scheme to the one reported in [26], [27] for the determination of the envelope function in microwave rotary encoders. The sketch of the whole sensor is depicted in Fig. 3. From the sensor design point of view, in order to enhance the sensitivity, it is convenient to bring the upper transmission zero (the most sensitive to variations in the dielectric constant of the MUT) close to the pole.

By doing this, the variation experienced by the transmission coefficient at f_0, with a change in the dielectric constant of the MUT, is expected to be stronger. That is, by approaching the upper transmission zero to the pole in the bare sensor structure, the excursion of the transmission coefficient at the operating frequency caused by the effects of the MUT is expected to be higher, thereby enhancing the sensitivity. Nevertheless, it should be mentioned that optimization of the sensitivity can be done at the expense of the reduction of the input dynamic range. To gain insight on this aspect, it suffices to consider the equivalent circuit model and two different cases. The difference in both cases concerns the position of the second transmission zero, the pole being located at roughly the same frequency.

In case (i), the second transmission zero is closer to the pole, thereby providing better sensitivity. This is corroborated in Fig. 4, where the responses achieved by modifying (increasing) the capacitance of the CSRR (equivalent to increase the dielectric constant of the MUT) are depicted. The variation of the transmission coefficient at $f_0 = f_p$ with the capacitance of the CSRR is stronger for case (i), but saturation (minimum value of transmission coefficient) is achieved for a smaller variation of such capacitance [corresponding to a smaller dynamic range as compared to case (ii)].

For a proper sensor design (including sensitivity optimization), it is convenient to know the approximate range of variation of the dielectric constants of the considered MUTs. Let us consider that the input dynamic range is in the range between the dielectric constant of air (the minimum possible one, i.e., $\varepsilon_{MUT,min} = 1$) and a certain maximum value $\varepsilon_{MUT,max}$. Sensitivity optimization for such a dynamic range is achieved when the upper transmission zero of the sensor loaded with the MUT with $\varepsilon_{MUT} = \varepsilon_{MUT,max}$ coincides with the pole of the bare sensor, that is,

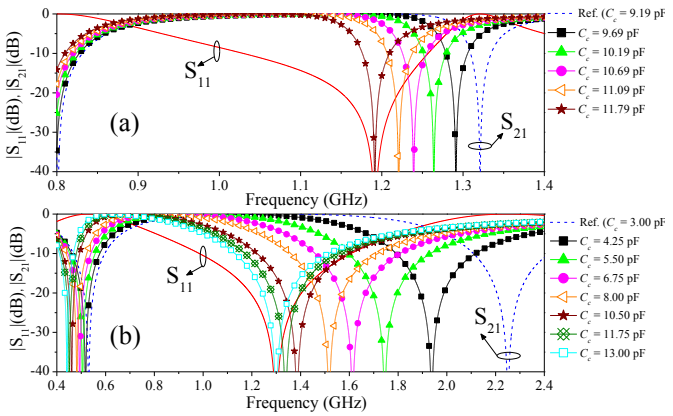

Fig. 4. Frequency responses inferred by circuit simulation of the circuit model by considering variations in the capacitance C_c of the CSRR. (a) L = 15.4 nH, C = 2.0 pF, L_c = 1.9 nH; (b) L = 3.1 nH, C = 10.0 pF, L_c = 5.1 nH. In both cases, Z_0 = 50 Ω and kl = 85º at f_0 = 1 GHz.

$$\omega_{p,bare} = \frac{1}{\sqrt{L_c C_{c,0}}} = \sqrt{\frac{LC + L_c C_{c,0} F + L_c C + \sqrt{\left(LC + L_c C_{c,0} F + L_c C\right)^2 - 4LCL_c C_{c,0} F}}{2LCL_c C_{c,0} F}} = \omega_{z,\varepsilon_{MUT,max}} \quad (5)$$

where $C_{c,0}$ is the capacitance of the unloaded CSRR. To clarify: if for the maximum value of the dielectric constant of the MUT in the considered input dynamic range, the transmission zero is translated to the pole of the bare sensor, where the operation frequency is tuned, this means that the excursion of the magnitude of the transmission coefficient is the maximum possible, therefore optimizing the sensitivity.

When the CSRR is loaded with a MUT (with dielectric constant ε_{MUT}), its capacitance changes to

$$C_c = C_{c,0} \frac{\varepsilon_r + \varepsilon_{MUT}}{\varepsilon_r + 1} \quad (6)$$

However, for simplification purposes, the following dimensionless factor has been used in (5)

$$F = \frac{\varepsilon_r + \varepsilon_{MUT,max}}{\varepsilon_r + 1} \quad (7)$$

i.e., $C_{c,\varepsilon MUT,max} = C_{c,0} \cdot F$ is the CSRR capacitance when this element is loaded with a MUT with $\varepsilon_{MUT} = \varepsilon_{MUT,max}$. It should be mentioned that the validity of (6) is subjected to the presence of MUTs with sufficient thickness, i.e., to guarantee that the electric field generated in the slots of the CSRR does not reach the MUT air interface (i.e., semi-infinite in the vertical direction). In addition, the area of the MUT should be enough to completely cover the region occupied by the CSRR, the sensitive element.

From (5), F can be isolated and expressed in terms of the reactive parameters as

$$F = 1 + \frac{L_c C}{LC - L_c C_{c,0}} \quad (8)$$

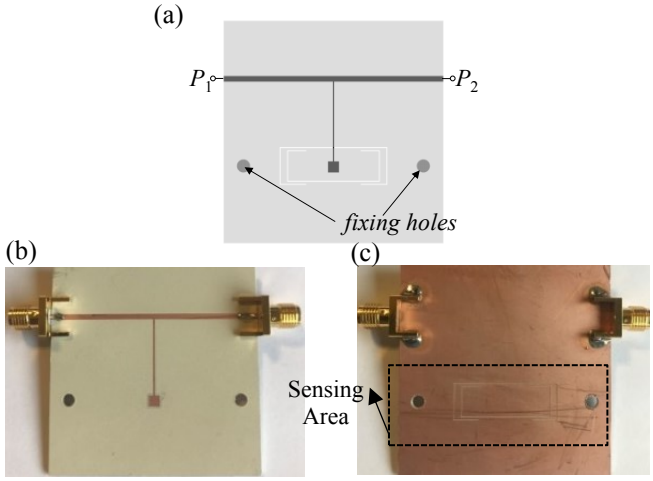

Fig. 5. Layout (a) and photograph of the top (b) and bottom (c) views of the fabricated sensor. Dimensions (in mm), in reference to Fig. 1(a), are: $l_{L_{SIR}}$ = 18.2, $l_{C_{SIR}}$ = $w_{C_{SIR}}$ = 2.5, $w_{L_{SIR}}$ = 0.2, l_{CSRR} = 8.6, w_{CSRR} = 24.6, c = 0.2, d = 1.5, g_{CSRR} = 12.4, L_{TL} = 50, and W_{TL} = 1.28 (50 Ω). The *Rogers RO3010* substrate with thickness h =1.27 mm and dielectric constant ε_r = 10.2 has been used for sensor implementation. Teflon screws are used in order to put pressure in the MUT against the CSRR, thereby minimizing the effects of the air gap present between the sensor and the MUT.

Thus, from the design point of view, given $\varepsilon_{MUT,max}$, the factor F should be calculated by means of (7), and the reactive parameters should be chosen in order to satisfy (8). Note that, according to (8), it is necessary that $LC > L_c C_{c,0}$. Otherwise, $F < 1$, and this is not possible since $\varepsilon_{MUT} > 1$. In other words, if $LC > L_c C_{c,0}$ is not satisfied, then the upper transmission zero cannot reach the pole of the bare sensor, even for $\varepsilon_{MUT,max} \to \infty$. In addition, according to (8), for enhancing the input dynamic range, it is necessary that LC does not differ excessively from $L_c C_{c,0}$.

The specific sensor designs of this paper (devoted to the characterization of both solid and liquid MUT samples, and left for the next section), have been carried out by considering the previous design guidelines, which are considered to be a relevant contribution of this paper.

IV. Experimental Validation

The main objective of the proposed approach is to demonstrate the potential of the sensor for liquid characterization. Nevertheless, let us first report the implementation of a prototype able to provide the dielectric constant of low-loss solid materials.

A. Measurement of the Dielectric Constant of Solid Samples

The first designed prototype sensor is devoted to the dielectric characterization of solid samples, where the maximum dielectric constant is $\varepsilon_{MUT,max}$ =10.2 (corresponding to the microwave substrate with higher dielectric constant among those available in our laboratory). Thus, we have designed the sensor in order to optimize the sensitivity and simultaneously achieve an input dynamic range of roughly [1-10.2]. For that purpose, the pole of the bare sensor, $f_{p,bare}$,

should roughly coincide with the upper transmission zero of the response of the sensor loaded with the MUT with $\varepsilon_{MUT} = \varepsilon_{MUT,max} = 10.2$, as indicated before.

The layout and photograph of the designed sensor are depicted in Fig. 5, where the relevant dimensions are indicated. With such dimensions and the considered substrate (the *Rogers RO3010* substrate with thickness $h = 1.27$ mm and dielectric constant $\varepsilon_r = 10.2$) the reactive element values are $L = 12.79$ nH, $C = 1.68$ pF, $L_c = 1.58$ nH, and $C_{c,0} = 12.25$ pF. Such element values roughly satisfy expression (8), with $F = 1.82$ [such value of F is obtained by means of (7) from the considered ε_r and $\varepsilon_{MUT,max}$ values]. The small discrepancy is attributed to the fact that the dimensions have been adjusted in order to obtain $f_{p,bare} = f_{z,MUT,max}$, but the considered MUTs actually exhibit a thickness of roughly 1.5 mm, i.e., below the required value for considering the MUTs semi-infinite in the vertical direction. Nevertheless, final dimensions tuning in order to optimize the sensitivity for the given input dynamic range (i.e, to force $f_{p,bare} = f_{z,MUT,max}$) is necessary. The reason is that, even though there are analytical expressions linking dimensions and reactive parameters for both the SIR [75] and the CSRR [76], such elements are not isolated in the reported structures. On the contrary, both elements constitute the so-called CSRR-loaded SIR composite resonator, and their proximity and interaction force us to determine the final dimensions by tuning.

It should be mentioned that the relatively high dielectric constant of the considered substrate provides small sensor size. However, in general, increasing the dielectric constant of the substrate penalizes sensor sensitivity. Nevertheless, in this paper, the main aim has been to demonstrate the potential of the reported approach for the implementation of small sized single-frequency sensors, and the considered substrate has been arbitrarily chosen among those available in our laboratory. Despite this fact, the obtained sensitivities are reasonable, as it will be shown later.

The simulated and measured responses for different materials are shown in Fig. 6, where it can be appreciated that $f_{p,bare}$ is very close to the upper transmission zero of the response with $\varepsilon_{MUT} = 10.2$, i.e., $f_{z,\,MUT,max}$. The figure includes the lossless electromagnetic and circuit simulation responses [Fig. 6(a)], where it can be appreciated that the model describes the lossless electromagnetically simulated responses to a good approximation. Nevertheless, it should be mentioned that for the responses corresponding to the MUTs with higher dielectric constant (*Rogers RO3010* and *MT-copper*), an additional transmission zero in the response inferred from the electromagnetic simulator is visible. Such zero is due to higher-order resonances of the composite resonator, and it is not accounted for by the circuit model, as far as it is considered to be a parasitic, i.e., out of interest and far enough from the operating frequency at $f_0 = f_{p,bare}$. It can be also seen that the excursion experienced by the transmission coefficient at $f_0 = f_{p,bare}$, when ε_{MUT} varies between 1 (air) and 10.2 (the higher dielectric constant substrate), is roughly 17 dB, with the maximum value (for $\varepsilon_{MUT} = 1$) at 0.8 dB.

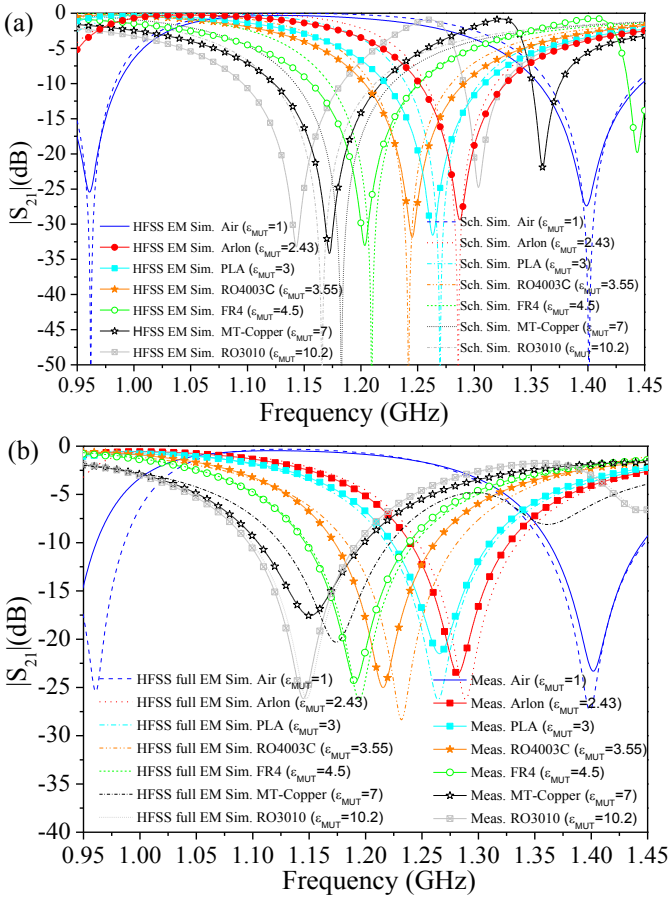

Fig. 6. Response of the sensor for different MUTs. (a) Circuit response of Fig. 1(b) inferred from the schematic simulator of *Keysight ADS* compared to the lossless electromagnetic simulation obtained by means of the *Ansys HFSS* electromagnetic solver; (b) Measured responses compared with the lossy electromagnetic simulations (also inferred by means of *Ansys HFSS*). In the circuit responses inferred from the *Keysight ADS* schematic simulator, the reactive parameters are those given in the text, and C_c given by (6) for the different values of ε_{MUT}.

It should be mentioned that operation of the sensor in the considered frequency obeys a tradeoff between sensor size (smaller as frequency increases) and simplicity of the associated electronics (including the generation of the harmonic signal) and post processing in a real scenario.

The next step has been to implement the whole sensor, including the feeding harmonic signal, tuned to $f_0 = f_{p,bare} = 1.125$ GHz, plus the envelope (AM) detector and the isolator. The feeding signal has been injected by means of a vector network analyzer (model *PNA N5221A*).

The envelope detector has been implemented by means of the high detection sensitivity *Avago HSMS-2860* Schottky diode (with threshold voltage $V_{F,max} = 150$ mV and operating frequency range between 0.91 GHz and 5.8 GHz) and the *Agilent N2795A* active probe (with capacitance and resistance $C = 1$ pF and $R = 1$ MΩ, respectively). Such active prove acts as the low pass filter needed to obtain the envelope function, and avoids the use of further lumped elements. Finally, the isolator has been implemented by means of the *ATM PNR ATc4-8* circulator.

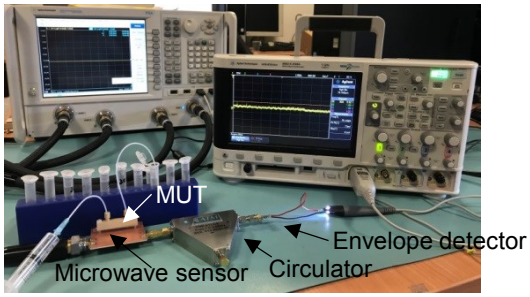

Fig. 7. Photograph of the experimental setup.

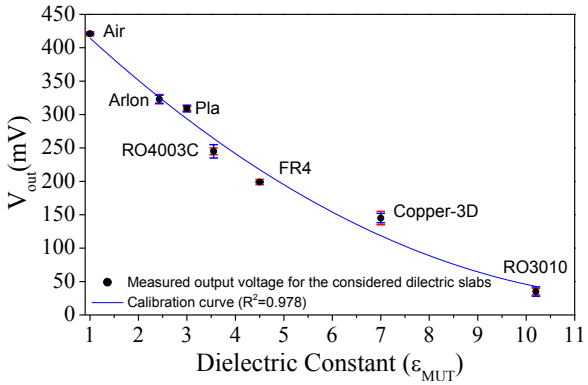

Fig. 8. Variation of the output signal of the sensor (amplitude level of the harmonic signal at the output port) as a function of the dielectric constant of the MUT, ε_{MUT}.

The potential mismatch caused by the detector circuitry does not affect the core of the sensor (the line loaded with the composite resonator), due to the effects of the circulator. Such component operates as an isolator, and thereby prevents from any potential mismatching reflection caused by the diode. The photograph of the whole experimental setup is shown in Fig. 7. Fig. 8 depicts the amplitude of the output signal, visualized in an oscilloscope (model *Agilent MSO-X 3104A*), as a function of the dielectric constant of the MUT.

From this data, a calibration curve can be inferred (included in Fig. 8), and used to determine the dielectric constant of any unknown MUT from the measurement of the amplitude voltage level. The maximum sensitivity, defined as the absolute value of the derivative of the output voltage with the dielectric constant of the MUT, is found to be 116.36 mV. It is interesting to highlight that sensing involves a simple measurement of the amplitude of the output signal by means of an envelope detector, and the interrogation signal for sensing is a single tone (harmonic) signal. It should be mentioned that three measurements for each sample have been carried out in order to ensure that the results are repetitive. The averaged value as well as the obtained error bars are included in Fig. 8.

B. Microfluidic sensor for liquid characterization

The second prototype is devoted to the characterization of liquid samples, particularly, to the determination of the solute content in solutions of isopropanol in DI water. The interest is the determination of the volume fraction of isopropanol in diluted solutions of DI water. Therefore, in this case, the sensor design procedure is slightly different from the previous case (solid samples). Let us consider that the input dynamic range is roughly 0-40% of volume fraction. Since the dielectric constant of water (≈ 80) is much larger than that of isopropanol (≈ 18), it follows that by increasing the volume fraction of isopropanol, the frequency response of the sensor should shift upwards. Thus, from the design viewpoint, the objective has been to force the second transmission zero of the response with pure DI water to coincide with the pole frequency of the response with a solution of 40% isopropanol.

The designed device (perspective views and photographs) is depicted in Fig. 9, whereas Fig. 10 depicts the electromagnetic simulations corresponding to pure DI water and considering a solution of 40% of isopropanol. As it can be seen, the above design criterion is satisfied, i.e., the second transmission zero of the response with pure DI water coincides to a good approximation with the pole of the response with a solution of 40% isopropanol. The experimental validation has been carried out by including a microfluidic channel on top of the CSRR, and the necessary mechanical accessories (including the capillaries for liquid injection by means of a syringe). The details of the fluidic part are given in [54] and summarized in the caption of Fig. 9. The measured responses of the sensor for pure DI water and a mixture of 40% of isopropanol in DI water, as well as for intermediate values of the isopropanol concentration are also included in Fig. 10. The agreement with the simulated curves (for pure DI water and 40% of isopropanol concentration, the simulated cases) is reasonable.

The next step has been to feed the sensor with a harmonic signal tuned to the frequency of the second transmission zero of the response with pure DI water. The amplitude voltage levels at the output port for different concentrations of isopropanol, inferred by means of the experimental setup depicted in Fig. 7, are depicted in Fig. 11 (the calibration curve is included in the figure). The maximum sensitivity is found to be 4 mV/%, and the device is able to resolve volume fractions as small as 5 %, a very competitive value. Similar to the characterization of solid samples, the fluidic measurements have been performed three times to verify the repeatability of the results (error bars are also included in Fig. 11).

V. Comparison to other approaches and discussion

There are several proposals of sensors devoted to the measurement of volume fraction of various components (i.e., methanol, ethanol or isopropanol) in DI water. These sensors and their main features are included in Table I (F_v in the table is the sensor resolution in volume fraction). Comparing such sensors is not easy, as far as they are based on different principles. It should be mentioned, however, that most sensors require wideband interrogation signals for measuring purposes, contrary to the sensor reported in this paper. This feature is also present in the sensor reported in [65], a differential-mode sensor based on a pair of meandered lines (the sensitive part) and a pair of rat-race hybrid couplers.

The couplers are used to transform the phase information to magnitude information. Nevertheless, the output variable in the sensor reported in [65] is the magnitude of the transmission coefficient between the input and the output ports.

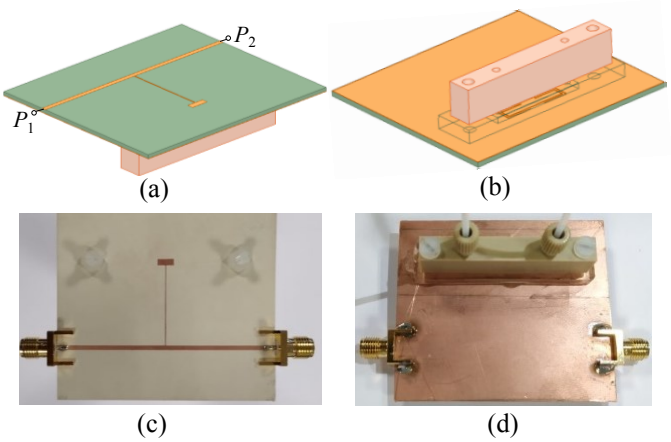

Fig. 9. Top (a) and bottom (b) perspective views and photographs of the top (c) and bottom (d) views of the fabricated sensor for liquid characterization. Dimensions (in mm), in reference to Fig. 1(a), are: $l_{L_{SIR}}$ = 22.0, $l_{C_{SIR}}$ = 1.9, $w_{C_{SIR}}$ = 5.4, $w_{L_{SIR}}$ = 0.2, l_{CSRR} = 4.4, w_{CSRR} = 18.6, c = 0.2, d = 0.5, g_{CSRR} = 4.3, L_{TL} = 60, and W_{TL} = 1.28 (50 Ω). The *Rogers RO3010* substrate with thickness h =1.27 mm and dielectric constant ε_r = 10.2 has been used. Channel dimensions are: length 26 mm, height 1.5 mm and width 4.6 mm, and the channels have been fabricated with polydimethylsiloxane (PDMS).

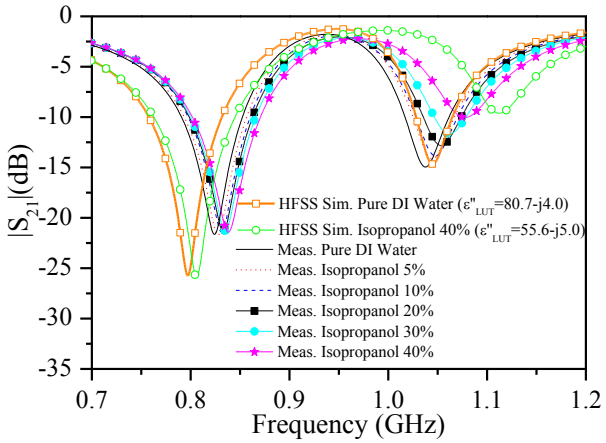

Fig. 10. Simulated transmission coefficient (using the *Ansys HFSS* electromagnetic solver) and measured responses of the sensor for the indicated volume fractions of isopropanol in DI water (the complex dielectric constants of the solutions with the extreme concentrations of isopropanol, i.e., 0% and 40%, are indicated).

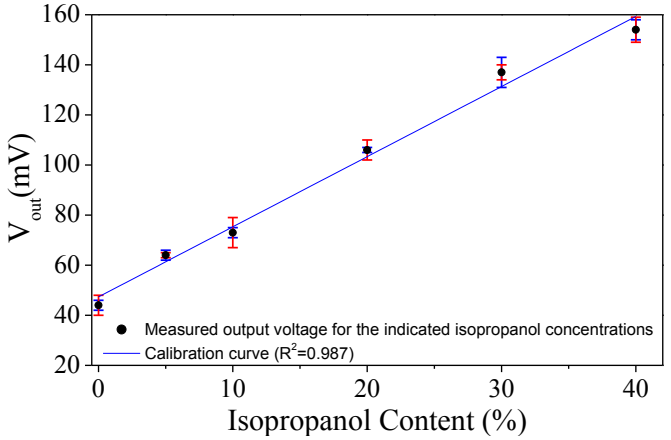

Fig. 11. Variation of the output signal of the sensor (amplitude level of the harmonic signal at the output port) as a function of the volume fraction of isopropanol.

TABLE I
COMPARISON OF VARIOUS MICROWAVE FLUIDIC SENSORS FOR VOLUME FRACTION MEASUREMENT IN LIQUID SOLUTIONS

Ref.	*Single-frequency*	F_V (%)	*Sensitivity*	*Size* (cm^2)	*Op./central freq.* (GHz)
[9]	NO	5	98 MHz/%	0.0023	20.0
[32]	NO	20	4 MHz/%	-	1.9
[37]	NO	10	1.5 MHz/%	2.56	1.9
[38]	NO	10	2.2 MHz/%	8.91	4.7
[54]	NO	10	0.5 MHz/%	53.32	0.95
[44]	NO	0.005	120 MHz/%	6.80	2.6
[59]*	YES	5	0.8 dB/%	35.06	0.9
[77]	NO	0.1	1 MHz/%	-	5.7
[78]	NO	10	1.75 MHz/%	7.75	2.4
[79]*	YES	20	0.02 dB/%	9.70	1.0
[80]	NO	10	0.54MHz/%	0.0026	0.64
[81]	YES	20	0.023dB/mg/mL	4.5	19.3
[82]	NO	---	13MHz	---	3.97
[83]	YES	---	0.025dB/mg/mL	---	1.91
[84]	YES	---	0.18dB/mg/mL	10.5	1.65
[85]	YES	---	0.01dB/mg/mL	23.04	3.41
[61]*	YES	5	0.33 dB/%	50.00	0.95
[65]	YES	1	11.52 dB/%	182.11	1.97
This work*	**YES**	**5**	**4 mV/% 0.33 dB/%**	**15.78**	**1.125**

*These sensors can also operate as frequency-variation sensors, but the reported sensitivity corresponds to their mode of operation as single-frequency sensors.

By contrast, in the sensor reported in this paper, the output variable is the amplitude of the signal present at the output port of the sensor, and inferred by means of an envelope detector. The resolution of the sensor of [65] is very good, but sensor dimensions are by far superior to those of the sensor reported in this paper. Concerning the sensitivity of the fluidic sensor reported in this paper, it is intimately related to the level of the feeding signal (1 mW in our case).

In order to compare the sensitivity of the sensor of Fig. 9 with the one of other single-frequency sensors where the output variable is the magnitude of the transmission coefficient, we have expressed the sensitivity from the variation experienced by the transmission coefficient with the percentage of isopropanol at f_0 (see Table I).

This sensitivity is an indicator of the capability of the sensor for detecting small changes in the magnitude of the input variable (volume fraction in our case). For sensitivity optimization, both the transmission coefficient span, as well as the maximum value should be high, a characteristic of the proposed sensor. In the sensor reported in [65], the excursion of the transmission coefficient at the operating frequency is roughly 50 dB, a very high value. However, the maximum value is small (roughly –20 dB). For the sensors reported in [59], [61], the output variable is the cross-mode transmission coefficient, and it exhibits an excursion of 22 dB and 25 dB, respectively, at the design frequency, with maximum values of –13 dB and –5 dB.

In the fluidic sensor of Fig. 9, the excursion of the transmission coefficient at the operating frequency is roughly 15 dB, with a maximum value close to 0 dB by virtue of the

pole. This combination of transmission coefficient excursion and maximum value is very interesting for sensitivity optimization in terms of V/%, and is achieved thanks to the unique features of the proposed sensor, with the presence of a transmission zero and a pole at closely spaced (and controllable) frequencies. Nevertheless, the sensitivity in V/% can be further enhanced by increasing the power of the input harmonic signal. Interestingly, the sensor response of Fig. 11 is roughly linear over the considered input dynamic range. Additionally, the size of the proposed sensor is very competitive.

It should be mentioned that the sensor of [80] exhibits also a very good combination of size and sensitivity, but it does not operate at a single frequency. Nevertheless, an excellent size was achieved in that sensor, which allows for nanodroplet detection. The sensor in [81] operates at a single frequency, and it measures the magnitude of the reflection coefficient, this being an interesting feature of this sensor. Nevertheless, in this sensor, the sensitivity is given in dB/mg/mL by the authors. Other sensors where the output variable is the magnitude of the transmission coefficient of a resonator-based structure are found in [83]-[85]. In such sensors, like in the device presented in [81] the input variable is the solute content (glucose) in mg/mL, therefore the comparison in terms of the sensitivity with other sensors where the solute materials are different types of alcohols, and where the input is expressed as volume fraction, is not simple.

Let us emphasize that by working at a single frequency, the reported sensor benefits from the low cost of the associated electronics necessary for the generation of the interrogation signal. In a real scenario, a fixed-frequency oscillator suffices for that purpose, and this represents a simple and low-cost solution, in comparison to the complexity and high cost of the wideband voltage controlled oscillators (VCOs) that are necessary in sensors based on frequency variation. It should be also mentioned that, for demonstration purposes, the output signal in the reported sensors has been visualized in an oscilloscope. Nevertheless, a simple and low-cost digital post-processing stage can replace the oscilloscope in a real scenario, thereby contributing to the competitiveness of the reported sensors in terms of cost. The envelope detector, based on discrete components, can also be replaced with an integrated demodulator module, inexpensive and with better performance. Nevertheless, these aspects are out of the scope of this paper, mainly devoted to the analysis and design of the microwave/microfluidic part of the sensor.

If necessary, the sensor can also operate as a frequency variation sensor, as far as the second transmission zero (frequency position and depth) is quite sensitive to the characteristics of the liquid sample. Under this mode of operation, determination of the dielectric constant and loss factor of the material under test is possible, similar to other sensors reported in the literature (e.g., [39]). However, the main purpose of this paper, as emphasized before, has been to demonstrate the possibility of implementing a single-frequency sensor able to monitor a material variable (volume fraction of a liquid mixture in our case) by means of a simple voltage-amplitude measurement. Other sensors that use wideband interrogation signals, based on non-resonant structures, and devoted to dielectric spectroscopy, have been reported in the literature (see, e.g., [86]-[90]). As compared to these sensors, the proposed sensors in this paper are simple, operate at a single frequency, and can be designed in order to optimize the sensitivity, given a certain input dynamic range. Indeed, these advantages are related to the fact that the proposed sensors are based on a resonant-type approach.

To end this section, let us mention that, in general, frequency modulation or phase modulation systems are more robust against noise or interference effects than amplitude modulation systems. However, measuring the amplitude of a voltage, the output variable of the proposed sensors, is simpler than measuring, e.g., a phase (there are single frequency sensors based on the measurement of the phase). Moreover, measuring the voltage amplitude at the operating frequency is even simpler than measuring the transmission coefficient. For that main reason, the proposed sensors, where voltage amplitude is obtained from an envelope detector system, are proposed. The results of Figs. 8 and 11 reveal that the sensors are useful for the measurement of the dielectric constant of solid samples, and for the determination of liquid composition in mixtures, with reasonable sensitivity. Moreover, the wideband responses in the vicinity of the pole frequency make the system tolerant against potential effects of detuning caused, e.g., by fabrication related tolerances, or by variations in temperature.

VI. Conclusion

In summary, a planar microwave sensor based on a composite resonator, i.e., a CSRR-loaded SIR, has been reported in this paper. The sensor is useful for microfluidic applications and for dielectric characterization of solid samples. Contrary to most sensors based on a single resonant element (based on frequency variation), the principle of operation of the proposed sensor is the variation of the transmission coefficient at a specific frequency. This is an important characteristic of the proposed sensor, since a wideband interrogation signal is not required for measuring purposes. Contrarily, it has been demonstrated that by feeding the sensor with a single-tone (harmonic) signal conveniently tuned, the amplitude of the output signal is dictated by the characteristics (dielectric constant) of the MUT, which should be in contact with the CSRR (the sensitive element). Therefore, the voltage amplitude of the output signal, obtained by means of a simple envelope (AM) detector, has been considered to be the output variable. Since the involved electronics necessary for sensing are simple, (mainly a harmonic oscillator in a real scenario and an envelope detector), the proposed sensor is competitive in terms of cost. Also, by virtue of the presence of a controllable pole and two transmission zeros in the CSRR-loaded SIR based line (the sensing structure), the achieved sensitivity and resolution is good. Particularly, the proposed microfluidic sensor is able to discriminate volume fractions of 5 % isopropanol in DI water, with a maximum measured sensitivity of 4 mV/%, i.e., very

competitive values. Application of the proposed sensor to industrial processes, such as the determination of percentage of alcohol in wine fermentation processes, is envisaged.

APPENDIX

SENSITIVITY OF THE TRANSMISSION ZERO FREQUENCIES WITH ε_{MUT}

This appendix demonstrates analytically that the upper transmission zero experiences a stronger variation with the dielectric constant of the MUT (ε_{MUT}) than the lower transmission zero. Since the single reactive parameter of the sensor depending on ε_{MUT} is the capacitance of the CSRR, C_c, the derivative of expression (2) with C_c should be calculated in order to determine which transmission zero is more sensitive to C_c, and consequently to ε_{MUT}. Nevertheless, it is simpler to calculate the derivative of the square of the transmission zeros with C_c. Therefore, we have calculated such derivative, and the result, after some calculation, is found to be:

$$\frac{d\omega_z^2}{dC_c} = \frac{\pm LCL_c^2C_c(-LC+L_cC_c+L_cC)A^{-\frac{1}{2}} - L^2C^2L_c - LC^2L_c^2 \mp LCL_cA^{\frac{1}{2}}}{2L^2C^2L_c^2C_c^2} \quad (A.1)$$

In (A.1), A is the square root in the numerator of (2), i.e.,

$$A = (LC + L_cC_c + L_cC)^2 - 4LCL_cC_c \quad (A.2)$$

and is used for simplification purposes. Moreover, the derivative of the square of the upper transmission zero is the one given by the upper sign, whereas the lower sign provides the derivative of the square of the lower transmission zero. Note that both derivatives in (A.1) should be negative, since the overall sensor response shifts down by increasing C_c, or ε_{MUT}.

A simple analysis of (A.1) reveals that the magnitude of the derivative of the square of the transmission zero is higher for the upper transmission zero if the following condition is satisfied:

$$LCL_cA^{\frac{1}{2}} > LCL_c^2C_c(-LC + L_cC_c + L_cC)A^{-\frac{1}{2}} \quad (A.3)$$

Expression (A.3) can be simplified to:

$$C(L + L_c)^2 + L_cC_c(L_c - L) > 0 \quad (A.4)$$

which is typically satisfied for reasonable values of the reactive parameters. Indeed, expression (A.4) can be rewritten as:

$$L(LC - L_cC_c) + CL_c^2 + 2LCL_c + C_cL_c^2 > 0 \quad (A.5)$$

Since it is necessary that $LC > L_cC_c$, as justified before, it is clear that (A.5) is positive. Thus, the derivative is larger for the square of the upper transmission zero. It can be then concluded that such transmission zero frequency is more sensitive to the effects of C_c, or ε_{MUT}.

Despite the fact that the proposed sensor is a single frequency device, and therefore the sensitivity of the transmission zeros with ε_{MUT} is not the relevant one, such sensitivity can be easily calculated as

$$\frac{d\omega_z}{d\varepsilon_{MUT}} = \frac{d\omega_z}{dC_c}\frac{dC_c}{d\varepsilon_{MUT}} = \frac{1}{2\omega_z}\frac{d\omega_z^2}{dC_c}\frac{dC_c}{d\varepsilon_{MUT}} = \frac{1}{2\omega_z}\frac{d\omega_z^2}{dC_c}\frac{C_{c,0}}{\varepsilon_r + 1} \quad (A.6)$$

REFERENCES

[1] G. Gennarelli, S. Romeo, M. R. Scarfì, and F. Soldovieri, "A Microwave Resonant Sensor for Concentration Measurements of Liquid Solutions", *IEEE Sensors J.*, vol. 13, pp. 1857-1864, May 2013.

[2] A. K. Jha and M. J. Akhtar, "A Generalized Rectangular Cavity Approach for Determination of Complex Permittivity of Materials", *IEEE Trans. Instrum. Meas.*, vol. 63, pp. 2632-2641, Nov. 2014.

[3] P. Wei, B. Morey, T. Dyson, N. McMahon, Y.-Y. Hsu, S. Gazman, L. Klinker, B. Ives, K. Dowling, C. Rafferty, "A Conformal Sensor for Wireless Sweat Level Monitoring", *2013 IEEE Sensors*, Baltimore, MD, USA, Nov. 2013.

[4] M. M. Rodgers, V. M. Pai, and R. S. Conroy, "Recent Advances in Wearable Sensors for Health Monitoring", *IEEE Sensors J.*, vol. 15, pp. 3119-3126, Jun. 2015.

[5] G. Galindo-Romera, F. J. Herraiz-Martínez, M. Gil, J. J. Martínez-Martínez, D. Segovia-Vargas, "Submersible printed split-ring resonator-based sensor for thin-film detection and permittivity characterization", *IEEE Sensors J.*, vol. 16, pp. 3587-3596, May 2016.

[6] A. Dehe, V. Krozer, K. Fricke, H. Klingbeil, K. Beilenhoff, and H.L. Hartnagel, "Integrated microwave power sensor", *Electron. Lett.*, vol. 31, pp. 2187-2188, Dec. 1995.

[7] J. Castillo-León, W. E. Svendsen, Lab-on-a-Chip Devices and Micro-Total Analysis Systems, *Springer*, Heidelberg, Germany, 2015.

[8] K. Grenier, D. Dubuc, P.-E. Poleni, M. Kumemura, H. Toshiyoshi, T. Fujii, and H. Fujita, "Integrated Broadband Microwave and Microfluidic Sensor Dedicated to Bioengineering", *IEEE Trans. Microw. Theory Techn.*, vol. 57, pp. 3246-3253, Dec. 2009.

[9] T. Chretiennot, D. Dubuc, K. Grenier, "A microwave and microfluidic planar resonator for efficient and accurate complex permittivity characterization of aqueous solutions", *IEEE Trans. Microw. Theory Techn.*, vol. 61 (2), pp. 972-978, 2012.

[10] A. Salim, S.H. Kim, J.Y. Park, S. Lim, "Microfluidic Biosensor Based on Microwave Substrate-Integrated Waveguide Cavity Resonator", *J. Sens.*, vol. 2018, 2018.

[11] M.H. Zarifi, H. Sadabadi, S.H. Hejazi, M. Daneshmand, A. Sanati-Nezhad, "Noncontact and Nonintrusive Microwave-Microfluidic Flow Sensor for Energy and Biomedical Engineering", *Sci. Rep.*, vol 8, article number 139, 2018.

[12] C. Mandel, B. Kubina, M. Schüßler, and R. Jakoby, "Passive chipless wireless sensor for two-dimensional displacement measurement," *41st Eur. Microw. Conf.*, Manchester, U.K., Oct. 2011, pp. 79–82.

[13] J. Naqui, M. Durán-Sindreu, and F. Martín, "Novel sensors based on the symmetry properties of split ring resonators (SRRs)," *Sensors*, vol. 11, no. 8, pp. 7545–7553, 2011.

[14] J. Naqui, M. Durán-Sindreu, and F. Martín, "On the symmetry properties of coplanar waveguides loaded with symmetric resonators: Analysis and potential applications," *IEEE MTT-S Int. Microw. Symp., Dig.*, Montreal, QC, Canada, Jun. 2012, pp. 1–3.

[15] J. Naqui, M. Durán-Sindreu, and F. Martín, "Alignment and position sensors based on split ring resonators," *Sensors*, vol. 12, no. 9, pp. 11790–11797, Aug. 2012.

[16] J. Naqui, M. M. Durán-Sindreu, and F. Martín, "Transmission lines loaded with bisymmetric resonators and applications," *IEEE MTT-S Int. Microw. Symp. Dig.*, Seattle, WA, USA, Jun. 2013, pp. 1–3.

[17] A. K. Horestani, C. Fumeaux, S. F. Al-Sarawi, and D. Abbott, "Displacement sensor based on diamond-shaped tapered split ring resonator," *IEEE Sensors J.*, vol. 13, no. 4, pp. 1153–1160, Apr. 2013.

[18] A. K. Horestani, D. Abbott, and C. Fumeaux, "Rotation sensor based on horn-shaped split ring resonator," *IEEE Sensors J.*, vol. 13, no. 8, pp. 3014–3015, Aug. 2013.

[19] J. Naqui and F. Martín, "Transmission lines loaded with bisymmetric resonators and their application to angular displacement and velocity sensors," *IEEE Trans. Microw. Theory Techn.*, vol. 61, no. 12, pp. 4700–4713, Dec. 2013.

[20] A. Ebrahimi, W. Withayachumnankul, S. F. Al-Sarawi, and D. Abbott, "Metamaterial-inspired rotation sensor with wide dynamic range," *IEEE Sensors J*., vol. 14, no. 8, pp. 2609–2614, Aug. 2014.

[21] A. K. Horestani, J. Naqui, Z. Shaterian, D. Abbott, C. Fumeaux, and F. Martín, "Two-dimensional alignment and displacement sensor based on movable broadside-coupled split ring resonators," *Sens. Actuator A, Phys.*, vol. 210, pp. 18–24, Apr. 2014.

[22] A. K. Horestani, J. Naqui, D. Abbott, C. Fumeaux, and F. Martín, "Two dimensional displacement and alignment sensor based on reflection coefficients of open microstrip lines loaded with split ring resonators," *Electron. Lett*., vol. 50, no. 8, pp. 620–622, Apr. 2014.

[23] J. Naqui and F. Martín, "Angular displacement and velocity sensors based on electric-LC (ELC) loaded microstrip lines," *IEEE Sensors J*., vol. 14, no. 4, pp. 939–940, Apr. 2014.

[24] J. Naqui, J. Coromina, A. Karami-Horestani, C. Fumeaux, and F. Martín, "Angular displacement and velocity sensors based on coplanar waveguides (CPWs) loaded with S-shaped split ring resonators (S-SRR)," *Sensors*, vol. 15, no. 5, pp. 9628–9650, 2015.

[25] J. Naqui and F. Martín, "Application of broadside-coupled split ring resonator (BC-SRR) loaded transmission lines to the design of rotary encoders for space applications," *IEEE MTT-S Int. Microw. Symp*., San Francisco, CA, USA, May 2016, pp. 1–4.

[26] J. Mata-Contreras, C. Herrojo, and F. Martín, "Application of split ring resonator (SRR) loaded transmission lines to the design of angular displacement and velocity sensors for space applications," *IEEE Trans. Microw. Theory Techn*., vol. 65, no. 11, pp. 4450–4460, Nov. 2017.

[27] J. Mata-Contreras, C. Herrojo, and F. Martín, "Detecting the Rotation Direction in Contactless Angular Velocity Sensors Implemented With Rotors Loaded With Multiple Chains of Resonators", *IEEE Sensors J*., vol. 18, pp. 7055-7065, Sep. 2018.

[28] C. Damm, *et al*., "Artificial transmission lines for high sensitive microwave sensors," *IEEE Sensors Conf*., Christchurch, New Zealand, 2009, pp. 755–758.

[29] F.J. Ferrández-Pastor, J.M. García-Chamizo and M. Nieto-Hidalgo, "Electromagnetic differential measuring method: application in microstrip sensors developing", *Sensors*, vol. 17, p. 1650, 2017.

[30] J. Muñoz-Enano, P. Vélez, M. Gil, F. Martín "An Analytical Method to Implement High Sensitivity Transmission Line Differential Sensors for Dielectric Constant Measurements", *IEEE Sensors J*., vol. 20, pp. 178-184, Jan. 2020.

[31] M. Puentes, *Planar Metamaterial Based Microwave Sensor Arrays for Biomedical Analysis and Treatment*, Springer: Heidelberg, Germany, 2014.

[32] A. Ebrahimi, W. Withayachumnankul, S. Al-Sarawi, and D. Abbott, "High-sensitivity metamaterial-inspired sensor for microfluidic dielectric characterization", *IEEE Sens. J.* vol. 14, pp. 1345–1351, May 2014.

[33] M. Schueler, C. Mandel, M. Puentes, and R. Jakoby, "Metamaterial inspired microwave sensors", *IEEE Microw. Mag*., vol. 13, pp. 57–68, 2012.

[34] M.S. Boybay, and O.M. Ramahi, "Material characterization using complementary split-ring resonators", *IEEE Trans. Instrum. Meas*., vol. 61, pp. 3039–3046, 2012.

[35] C.S. Lee, C.L. Yang, "Complementary split-ring resonators for measuring dielectric constants and loss tangents", *IEEE Microw. Wirel. Compon. Lett*., vol 24, pp. 563–565, 2014.

[36] C.L. Yang, C.S. Lee, K.W. Chen, K.Z. Chen, "Noncontact measurement of complex permittivity and thickness by using planar resonators", *IEEE Trans. Microw. Theory Tech.*, vol. 64, pp. 47–257, 2016.

[37] W. Withayachumnankul, K. Jaruwongrungsee, A. Tuantranont, C. Fumeaux, and D. Abbott, "Metamaterial-based microfluidic sensor for dielectric characterization", *Sens. Actuators A Phys*., vol. 189, pp. 233–237, 2013.

[38] A. Salim, and S Lim, "Complementary split-ring resonator-loaded microfluidic ethanol chemical sensor", *Sensors*, vol. 16, p. 1802, 2016.

[39] L. Su, J. Mata-Contreras, P. Vélez, A. Fernández-Prieto, and F. Martín, "Analytical method to estimate the complex permittivity of oil samples", *Sensors*, vol., 18, p. 984, 2018.

[40] M. Abdolrazzaghi, M.H. Zarifi, and M. Daneshmand, "Sensitivity enhancement of split ring resonator based liquid sensors", *2016 IEEE Sensors*, 1-3, Nov. 2016.

[41] M. Abdolrazzaghi, M.H. Zarifi, W. Pedrycz, M. Daneshmand, "Robust ultra-high resolution microwave planar sensor using fuzzy neural network approach", *IEEE Sensors* J., vol. 17 (2), pp. 323-332, Jan. 2017.

[42] M.H. Zarifi, M. Daneshmand, "Monitoring solid particle deposition in lossy medium using planar resonator sensor", *IEEE Sensors J*., vol. 17 (23), pp. 7981-7989, 2017.

[43] M.H. Zarifi, S. Deif, M. Abdolrazzaghi, B. Chen, D. Ramsawak, M. Amyotte, "A microwave ring resonator sensor for early detection of breaches in pipeline coatings", *IEEE Trans. Ind. Electron*., vol. 65 (2), pp. 1626-1635, 2017.

[44] M. Abdolrazzaghi, M. Daneshmand, A.K. Iyer, "Strongly enhanced sensitivity in planar microwave sensors based on metamaterial coupling", *IEEE Trans. Microw. Theory Techn*., vol. 66 (4), pp. 1843-1855, Apr. 2018.

[45] M.H Zarifi, H. Sadabadi, S.H. Hejazi, M. Daneshmand, A. Sanati-Nezhad, "Noncontact and nonintrusive microwave-microfluidic flow sensor for energy and biomedical engineering", *Sci. Rep*., vol. 8 (1), p. 139, 2018.

[46] A. Ebrahimi, J. Scott, K. Ghorbani, "Ultrahigh-Sensitivity Microwave Sensor for Microfluidic Complex Permittivity Measurement", *IEEE Trans. Microw. Theory Techn.*, vol. 67 (10), pp. 4269-4277, 2019.

[47] J. Naqui, C. Damm, A. Wiens, R. Jakoby, L. Su, and F. Martín, "Transmission lines loaded with pairs of magnetically coupled stepped impedance resonators (SIRs): modeling and application to microwave sensors," *IEEE MTT-S Int. Microw. Symp*. *Dig.*, Tampa, FL, USA, Jun. 2014, pp. 1–4.

[48] L. Su, J. Naqui, J. Mata-Contreras, and F. Martín "Modeling metamaterial transmission lines loaded with pairs of coupled split ring resonators," *IEEE Antennas Wirel. Propag. Lett.*, vol. 14, pp. 68–71, 2015.

[49] L. Su, J. Naqui, J. Mata, F. Martín, "Dual-band epsilon-negative (ENG) transmission line metamaterials based on microstrip lines loaded with pairs of coupled complementary split ring resonators (CSRRs): modeling, analysis and applications", *9th Int. Congress Adv. Electromagn. Mat. Microw. Opt.*, Metamaterials'2015, Oxford, UK, Sep., 7-12, 2015.

[50] L. Su, J. Naqui, J. Mata-Contreras, P. Vélez, F. Martín, "Transmission line metamaterials based on pairs of coupled split ring resonators (SRRs) and complementary split ring resonators (CSRR): a comparison to the light of the lumped element equivalent circuits", *Int. Conf. Electromagn. Adv. Applications*, ICEAA 2015, Torino, Italy, 7-11 Sep. 2015.

[51] L. Su, J. Naqui, J. Mata-Contreras, and F. Martín, "Modeling and applications of metamaterial transmission lines loaded with pairs of coupled complementary split ring resonators (CSRRs)," *IEEE Antennas Wirel. Propag. Lett.*, vol. 15, pp. 154–157, 2016.

[52] J. Naqui, C. Damm, A. Wiens, R. Jakoby, L. Su, J. Mata-Contreras, and F. Martín, "Transmission Lines Loaded with Pairs of Stepped Impedance Resonators: Modeling and Application to Differential Permittivity Measurements", *IEEE Trans. Microw. Theory Techn*., vol. 64, no. 11, pp. 3864-3877, Nov. 2016.

[53] L. Su, J. Mata-Contreras, J. Naqui, and F. Martín, "Splitter/combiner microstrip sections loaded with pairs of complementary split ring resonators (CSRRs): modeling and optimization for differential sensing applications," *IEEE Trans. Microw. Theory Techn*., vol. 64, pp. 4362-4370, Dec. 2016.

[54] P. Vélez, L. Su, K. Grenier, J. Mata-Contreras, D. Dubuc, and F. Martín, "Microwave microfluidic sensor based on a microstrip splitter/combiner configuration and split ring resonators (SRR) for dielectric characterization of liquids", *IEEE Sensors J*., vol. 17, pp. 6589-6598, Aug. 2017.

[55] A. Ebrahimi, J. Scott, K. Ghorbani, "Differential sensors using microstrip lines loaded with two split-ring resonators", *IEEE Sensors J*., vol. 18 (14), pp. 5786-5793, Jul. 2018.

[56] J. Naqui and F. Martín, "Microwave sensors based on symmetry properties of resonator-loaded transmission lines: a review," *J. Sensors*, vol. 2015, Article ID 741853, 10 pages, 2015.

[57] M. Gil, P. Vélez, F. Aznar, J. Muñoz-Enano, and F. Martín, "Differential sensor based on electro-inductive wave (EIW) transmission lines for dielectric constant measurements and defect detection", *IEEE Trans. Antennas Propag*., vol. 68, pp. 1876-1886, Mar. 2020.

[58] D. Shi, J. Guo, L. Chen, C. Xia, Z. Yu, Y. Ai, C.M. Li, Y. Kang, and Z. Wang, "Differential microfluidic sensor on printed circuit board for biological cells analysis", *Electrophoresis*., vol. 36(16), pp. 1854-1858, Aug. 2015.

[59] P. Vélez, K. Grenier, J. Mata-Contreras, D. Dubuc, and F. Martín, "Highly-sensitive microwave sensors based on open complementary split ring resonators (OCSRRs) for dielectric characterization and solute

concentration measurements in liquids", *IEEE Access*, vol. 6, pp. 48324-48338, Dec. 2018.
[60] P. Vélez, J. Muñoz-Enano, K. Grenier, J. Mata-Contreras, D. Dubuc, F. Martín, "Split ring resonator (SRR) based microwave fluidic sensor for electrolyte concentration measurements", *IEEE Sensors J*., vol. 19, no. 7, pp. 2562-2569, Apr. 2019.
[61] P. Vélez, J. Muñoz-Enano, M. Gil, J. Mata-Contreras, and F. Martín, "Differential microfluidic sensors based on dumbbell-shaped defect ground structures in microstrip technology: analysis, optimization, and applications", *Sensors*, vol. 19(14), p. 3189, 2019.
[62] J. Muñoz-Enano, P. Vélez, M. Gil, J. Mata-Contreras, and F. Martín, "Microwave Comparator based on Defect Ground Structures", *1st European Microwave Conference in Central Europe*, Prague, Czech Republic, May 13-15 2019.
[63] P. Vélez, J. Muñoz-Enano, F. Martín, "Electrolyte concentration measurements in DI water with 0.125g/L resolution by means of CSRR-based structures", *49th European Microwave Conference*, Paris, France, Sep.-Oct. 2019.
[64] J. Muñoz-Enano, P. Vélez, J. Mata-Contreras, M. Gil, D. Dubuc, K. Grenier, F. Martín, "Microwave Sensors/Comparators with Optimized Sensitivity Based on Microstrip Lines Loaded with Open Split Ring Resonators (OSRRs)", *49th European Microwave Conference*, Paris, France, Sep.-Oct. 2019.
[65] J. Muñoz-Enano, P. Vélez, M. Gil, J. Mata-Contreras, F. Martín, "Differential-mode to common-mode conversion detector based on rat-race hybrid couplers: analysis and application to microwave sensors and comparators", *IEEE Trans. Microw. Theory Techn*., vol. 68, no. 4, pp. 1312-1325, Apr. 2020.
[66] J. Muñoz-Enano, P. Vélez, M. Gil, and F. Martín, "Microfluidic reflective-mode differential sensor based on open split ring resonators (OSRRs)", *Int. J. Microw. Wirel. Technol*., vol. 12, pp. 588-597, Sep. 2020.
[67] A. Ebrahimi, J. Scott, K. Ghorbani, "Transmission Lines Terminated With LC Resonators for Differential Permittivity Sensing", *IEEE Microw. Wirel. Compon. Lett.*, vol. 28 (12), pp. 1149-1151, Dec. 2018.
[68] A. Ebrahimi, J. Scott, K. Ghorbani, "Microwave reflective biosensor for glucose level detection in aqueous solutions", *Sens. Actuators, A*, vol. 301, p. 111662, Jan 2020.
[69] P. Vélez, J. Muñoz-Enano, F. Martín, "Differential sensing based on quasi-microstrip-mode to slot-mode conversion", *IEEE Microw. Wirel. Compon. Lett.*, vol. 29, pp. 690-692, Oct. 2019.
[70] J. Naqui, *Symmetry Properties in Transmission Lines Loaded with Electrically Small Resonators: Circuit Modeling and Applications*, Springer, Heidelberg, Germany, 2016.
[71] F. Martín, *Artificial Transmission Lines for RF and Microwave Applications*, John Wiley, Hoboken, NJ, 2015.
[72] P. Vélez *et al*., "Step Impedance Resonator (SIR) Loaded with Complementary Split Ring Resonator (CSRR): Modeling, Analysis and Applications", *IEEE-MTT-S Int. Microw. Symp*. *Dig*., Los Angeles, CA, Jun. 2020.
[73] J. Naqui, M. Durán-Sindreu, J. Bonache and F. Martín, "Implementation of shunt connected series resonators through stepped-impedance shunt stubs: analysis and limitations", *IET Microw. Antennas Propag*., vol. 5, pp. 1336-1342, Aug. 2011.
[74] R. A. Foster, "A reactance theorem," *Bell Syst. Tech. J*., vol. 3, pp.259–267, Apr. 1924.
[75] D. M. Pozar, *Microwave Engineering*, Boston, MA, Addison Wesley, 1990.
[76] J.D. Baena, J. Bonache, F. Martín, R. Marqués, F. Falcone, T. Lopetegi, M.A.G. Laso, J. García, I Gil, M. Flores-Portillo and M. Sorolla, "Equivalent circuit models for split ring resonators and complementary split rings resonators coupled to planar transmission lines", *IEEE Trans. Microw. Theory Techn.*, vol. 53, pp. 1451-1461, Apr. 2005.
[77] B. D. Wiltshire and M. H. Zarifi, "3-D Printing Microfluidic Channels With Embedded .Planar Microwave Resonators for RFID and Liquid Detection," *IEEE Microw. Wirel. Compon. Lett.*, vol. 29, no. 1, pp. 65-67, Jan. 2019.
[78] X. Zhang, C. Ruan, T. ul Haq, and K. Chen, "High-Sensitivity Microwave Sensor for Liquid Characterization Using a Complementary Circular Spiral Resonator", *Sensors*, vol. 19. Feb. 2019.
[79] J. Kilpijärvi, N. Halonen, J. A. Juuti, and J. Hannu, "Microfluidic Microwave Sensor for Detecting Saline in Biological Range", *Sensors*, vol.19, Feb. 2019.
[80] S. Mohammadi and M. H. Zarifi, "DROP: A CMOS Differential Ring-Oscillator Sensing Platform for Nano-Liter Droplet Detection," *IEEE Transactions on Industrial Electronics*, doi: 10.1109/TIE.2020.3029466.
[81] S. Mohammadi *et al*., "Gold Coplanar Waveguide Resonator Integrated With a Microfluidic Channel for Aqueous Dielectric Detection," *IEEE Sensors J.*, vol. 20, no. 17, pp. 9825-9833, Sep. 2020.
[82] M. Amirian, G. Karimi, B. D. Wiltshire and M. H. Zarifi, "Differential Narrow Bandpass Microstrip Filter Design for Material and Liquid Purity Interrogation," *IEEE Sensors J.*, vol. 19, no. 22, pp. 10545-10553, Nov. 2019.
[83] G. Gennarelli, S. Romeo, M. R. Scarfi, and F. Soldovieri, "A microwave resonant sensor for concentration measurements of liquid solutions," *IEEE Sensors J*., vol. 13, no. 5, pp. 1857–1864, May 2013.
[84] S. Y. Huanget al., "Microstrip line-based glucose sensor for noninvasive continuous monitoring using the main field for sensing and multivariable crosschecking," *IEEE Sensors J*., vol. 19, no. 2, pp. 535–547, Jan. 2019.
[85] S. Harnsoongnoen and A. Wanthong, "Coplanar waveguide transmission line loaded with electric-LC resonator for determination of glucose concentration sensing," *IEEE Sensors J.*, vol. 17, no. 6, pp. 1635–1640, Mar. 2017.
[86] G. R. Facer, D. A. Notterman, and L. L. Sohn, "Dielectric spectroscopy for bioanalysis: From 40 Hz to 26.5 GHz in a microfabricated wave guide," *Appl. Phys. Lett*., vol. 78, no. 7, pp. 996.998, Feb. 2001.
[87] J. C. Booth, N. D. Orloff, J. Mateu, M. Janezic, M. Rinehart, and J. A. Beall, "Quantitative Permittivity Measurements of Nanoliter Liquid Volumes in Microfluidic Channels to 40 GHz," *IEEE Trans. Instrum. Meas*., vol. 59, no. 12, pp. 3279-3288, Dec. 2010.
[88] X. Ma, N. D. Orloff, C. A. E. Little, C. J. Long, I. E. Hanemann, S. Liu, J. Mateu, J. C. Booth, and J. C. M. Hwang, "A Multistate Single-Connection Calibration for Microwave Microfluidics," *IEEE Trans. Microw. Theory Techn.*, vol. 66, no. 2, pp. 1099-1107, Feb. 2018.
[89] S. Afshar, E. Salimi, K. Braasch, M. Butler, D. J. Thomson, and G. E. Bridges, "Multi-Frequency DEP Cytometer Employing a Microwave Sensor for Dielectric Analysis of Single Cells," *IEEE Trans. Microw. Theory Techn.*, vol. 64, no. 3, pp. 991-998, Mar. 2016.
[90] H. Li, Z. Chen, N. Borodinov, Y. Shao, I. Luzinov, G. Yu, and P. Wang, "Multi-Frequency Measurement of Volatile Organic Compounds with a Radio-Frequency Interferometer," *IEEE Sensors J*., vol. 17, no. 11, pp. 3323-3331, Jun. 2017.

Paris Vélez (S'10–M'14) was born in Barcelona, Spain, in 1982. He received the Degree in telecommunications engineering, specializing in electronics, the Degree in electronics engineering, and the Ph.D. degree in electrical engineering from the Autonomous University of Barcelona, Barcelona, in 2008, 2010, and 2014, respectively. His Ph.D. thesis was on common-mode suppression differential microwave circuits based on metamaterial concepts and semilumped resonators. He received the Pre-Doctoral Teaching and Research Fellowship from the Spanish Government from 2011 to 2014, during his PhD study. From 2015 to 2017, he was involved in subjects related to metamaterial sensors for fluidics detection and characterization at LAAS-CNRS through a TECNIOSpring fellowship, co-funded by the Marie Curie Program. Actually, he is a recipient of Juan de la Cierva fellowship. His current research interests include the miniaturization of passive RF/microwave circuits and metamaterial-based sensors. Dr. Vélez is a Reviewer of the IEEE TRANSACTIONS ON MICROWAVE THEORY AND TECHNIQUES and other microwave and sensor journals.

Jonathan Muñoz-Enano was born in Mollet del Vallès (Barcelona) Barcelona, Spain, in 1994. He received the Bachelor's Degree in Electronic Telecommunications Engineering in 2016 and the Master's Degree in Telecommunications Engineering in 2018, both at the Autonomous University of Barcelona (UAB). Actually, he is working in the same university in the elaboration of his PhD, which is focused on the development of microwave sensors based on metamaterials concepts for the dielectric characterization of materials and biosensors.

Amir Ebrahimi the Ph.D. degree from The University of Adelaide, Adelaide, SA, Australia, in 2016. He was a Visiting Research Fellow with Nanyang Technological University (NTU), Singapore, from 2014 to 2015. He is currently a Post-Doctoral Researcher with the School of Engineering, RMIT University, Melbourne, VIC, Australia. His research interests include metamaterial-inspired microwave devices, microwave circuit design, microwave filters, frequency-selective surfaces (FSSs) and nonlinear RF, and microwave circuit design and analysis.

Dr. Ebrahimi was a recipient of the YarmanCarlin Best Student Paper Award at the Mediterranean Microwave Symposium in 2015, the Best Student Paper at the Australian Microwave Symposium in 2016, He is a Reviewer for several recognized international journals, such as IEEE TRANSACTIONS ON MICROWAVE THEORY AND TECHNIQUES, and IEEE MICROWAVE AND WIRELESS COMPONENTS LETTERS.

Cristian Herrojo was born in Barcelona, Spain, in 1983. He received the Telecommunications Technical Engineering degree in electronic systems and Telecommunications Engineering degree from the Universitat Autònoma de Barcelona in 2010 and 2012, respectively and the PhD degree in Electronics Engineering from the same university in 2018. His research interests include RF/microwave devices, Chipless-RFID and RFID technology, and Metamaterials.

Ferran Paredes was born in Badalona (Barcelona), Spain in 1983. He received the Telecommunications Engineering Diploma (specializing in Electronics) and the Telecommunications Engineering degree from the Universitat Autònoma de Barcelona in 2004 and 2006, respectively and the PhD degree in Electronics Engineering from the same university in 2012. He was Assistant Professor from 2006 to 2008 at the Universitat Autònoma de Barcelona, where he is currently working as a Research Assistant. His research interests include metamaterial concepts, passive microwaves devices, antennas and RFID.

James Scott received the B.Eng. (Hons.) and M.Eng. (by research) degrees from the Royal Melbourne Institute of Technology, Melbourne, VIC, Australia, in 1979 and 1983, respectively, and the Ph.D. degree from the University of Melbourne in 2003. From 1981 to 1982, he was a Microwave and RF Design Engineer with Consolidated Technology (Aust.) Pty. Ltd., working on radar navigation systems. In 1982, he undertook his Ph.D. studies at the University of Melbourne. In 1987, he joined the Department of Communication and Electronic Engineering (now the School of Engineering), RMIT University, where he is currently the Associate Dean of electronic and telecommunications engineering. His research interests include radar systems, RF energy harvesting, nonlinear device modeling, and active and passive circuit design and simulation. He was the Inaugural Chair of the Joint MTT-S/ AP-S Chapter in the Victorian Section of the IEEE in 1998 and was the Student Activities Chair of the Victorian Section Committee from 1999 to 2003. He was served on the Organizing Committee of the Asia Pacific Microwave Conference, APMC 2011, which was held in Melbourne. He is a Reviewer of the IEEE TRANSACTIONS ON COMPONENTS, PACKAGING and the IEEE TRANSACTIONS ON MICROWAVE THEORY.

Kamran Ghorbani received the B.Eng (Hons.) and Ph.D. degrees from RMIT University, Melbourne, VIC, Australia, in 1994 and 2001, respectively. From 1994 to 1996, he was a Graduate RF Engineer with AWA Defence Industries, working on early warning radar systems. In 1996, he joined RMIT University to pursue his Ph.D. studies. From 1999 to 2001, he was a Senior RF Engineer with Tele-IP, working on VHF transceivers for commercial aircraft. In 2001, he joined the Department of Communication and Electronic Engineering (now the School of Engineering), RMIT University, as a continuing Academic. He is currently the Director of the Communication Technologies Research Centre, RMIT University. He is responsible for strategic planning and managing the research center. His research interests include dielectric measurements, composite material structures, frequency-selective surfaces, metamaterials, RF energy harvesting, radar systems, ferroelectric devices, and multifunctional antennas. Dr. Ghorbani is a voting member of the IEEE MTT-S Administrative Committee. He was the Chair of the Asia Pacific Microwave Conference, APMC 2011, which was held in Melbourne, Australia. He was the Co-Chair of the Technical Program Committee for the IEEE International Microwave and RF Conference, IMaRC 2014, which was held in India. He was also the Chair of the first Australian Microwave Symposium, AMS 2014, which was held in Melbourne, and the Technical Program Committee of the Asia Pacific Microwave Conference, APMC 2016, which was held in India. He served as an Associate Editor of IEEE TRANSACTIONS ON MICROWAVE THEORY AND TECHNIQUES and IET Microwaves, Antennas & Propagation.

Ferran Martín (M'04-SM'08-F'12) was born in Barakaldo, Spain, in 1965. He received the B.S. degree in physics and Ph.D. degree from the Universitat Autònoma de Barcelona (UAB), Barcelona, Spain, in 1988 and 1992, respectively. From 1994 to 2006 he was Associate Professor in Electronics at the Departament d'Enginyeria Electrònica (Universitat Autònoma de Barcelona), and since 2007 he is Full Professor of Electronics. His research activity has been very broad, including the modelling and simulation of electron devices for high frequency applications, millimeter wave and THz generation systems, the application of electromagnetic bandgaps to microwave and millimeter wave circuits, and the application of metamaterial concepts to the miniaturization and optimization of microwave circuits and antennas. He is now very active in the development of microwave sensors for dielectric characterization and motion control, and also in the topic of chipless-RFID. He is the head of the Microwave Engineering, Metamaterials and Antennas Group (GEMMA Group) at UAB, and director of CIMITEC, a research Center on Metamaterials supported by TECNIO (Generalitat de Catalunya). He has organized several international events related to metamaterials, including Workshops at the IEEE International Microwave Symposium (years 2005 and 2007) and European Microwave Conference (years 2009, 2015, 2017, and 2018), and the Fifth International Congress on Advanced Electromagnetic Materials in Microwaves and Optics (Metamaterials 2011), where he has acted as chair of the Local Organizing Committee. He has acted as Guest Editor in several Special Issues, mainly related to Metamaterials, in various International Journals. He has authored and co-authored over 650 technical conference, letter, journal papers and book chapters, he is co-author of the book on Metamaterials entitled *Metamaterials with Negative Parameters: Theory, Design and Microwave Applications* (John Wiley & Sons Inc. 2008), author of the book *Artificial Transmission Lines for RF and Microwave Applications* (John Wiley & Sons Inc. 2015), co-editor of the book *Balanced Microwave filters* (John Wiley & Sons Inc. and IEEE-Press 2018), and co-author of the book *Time Domain Signature Barcodes for Chipless-RFID and Sensing Applications* (Springer, 2020). Ferran Martín has generated 21 PhDs, has filed several patents on metamaterials and related concepts, and has headed several development contracts.

Prof. Martín is a member of the IEEE Microwave Theory and Techniques Society (IEEE MTT-S), member of the European Microwave Association (EuMA), and member of the Institution of Electronics and Technology (IET). He is reviewer of dozens of journals, including IEEE journals such as IEEE Transactions on Microwave Theory and Techniques, IEEE Microwave and Wireless Components Letters, and IEEE Sensors Journal, among others, and he serves as member of the Editorial Board of IET Microwaves, Antennas and Propagation and International Journal of RF and Microwave Computer-Aided Engineering. He is also a member of the Technical Committees of the European Microwave Conference (EuMC) and International Congress on Advanced Electromagnetic Materials in Microwaves and Optics (Metamaterials). Among his distinctions, Ferran Martín has received the 2006 Duran Farell Prize for Technological Research, he holds the *Parc de Recerca UAB – Santander* Technology Transfer Chair, and he has been the recipient of three ICREA ACADEMIA Awards (calls 2008, 2013 and 2018). He is Fellow of the IEEE since 2012 and Fellow of the IET since 2016.